Optical-feedback cavity-enhanced absorption spectroscopy for OH radical detection at 2.8 µm using a DFB diode laser

NANA YANG,[1,2] BO FANG,[1] WEIXIONG ZHAO,[1,5] (iD)
CHUNHUI WANG,[1,2] FEIHU CHENG,[1] XIAO HU,[1,2] YANG CHEN,[1,2]
WEIJUN ZHANG,[1,2,6] WEIGUANG MA,[3] (iD) GANG ZHAO,[3] (iD)
AND WEIDONG CHEN[4]

[1]*Laboratory of Atmospheric Physico-Chemistry, Anhui Institute of Optics and Fine Mechanics, HFIPS, Chinese Academy of Sciences, Hefei 230031, Anhui, China*
[2]*University of Science and Technology of China, Hefei 230026, Anhui, China*
[3]*State Key Laboratory of Quantum Optics & Quantum Optics Devices, Institute of Laser Spectroscopy, Shanxi University, 030006 Taiyuan, China*
[4]*Laboratoire de Physicochimie de l'Atmosphère, Université du Littoral Côte d'Opale, 59140 Dunkerque, France*
[5]*wxzhao@aiofm.ac.cn*
[6]*wjzhang@aiofm.ac.cn*

Abstract: We report the development of an optical-feedback cavity-enhanced absorption spectroscopy (OF-CEAS) instrument for OH detection at 2.8 µm using a DFB diode laser. Two different approaches, symmetry analysis and wavelength modulation, were performed to achieve laser frequency locking to the cavity mode. Compared with the symmetry analysis method, the wavelength modulation method continuously locked the laser frequency to the cavity mode and eliminated decoupling the laser from the cavity mode. A detection sensitivity of 1.7×10^{-9} cm^{-1} was achieved in a 25 s sampling time and was about 3 times better than that of the symmetry analysis method. The corresponding OH detection limit was ∼ 2×10^{8} molecule/cm³. Further improvement can be achieved by using higher reflectivity mirrors and other high-sensitivity approaches, such as frequency modulation spectroscopy and Faraday rotation spectroscopy.

1. Introduction

The hydroxyl radical (OH) plays crucial roles in atmospheric chemistry. The reaction between OH and methane (CH_4) determines the removal of atmospheric CH_4, which, as an important greenhouse gas, will have an important impact on atmospheric radiative forcing and global warming. The reactions between OH and volatile organic compounds (VOCs) and other trace pollutants determine the atmospheric self-cleaning capacity and the formation of secondary pollutants (e.g., ozone, photochemical smog, and secondary organic aerosols), all of which have a significant impact on the composition of the atmosphere, radiative forcing, and human health [1,2].

In situ direct measurement of atmospheric OH concentration with laser spectroscopy has long been a goal but is challenging due to the short lifetime (≤1s) and very low concentration (daily maximum concentration in the range of 10^6-10^7 molecule cm^{-3}) [1]. A detection limit of ∼ 10^5-10^6 molecule cm^{-3} is required for ambient air measurement. So far, only two spectroscopic methods, laser-induced fluorescence spectroscopy at low pressure (FAGE) and long-path differential optical absorption spectroscopy (DOAS), have been successfully employed.

The FAGE instruments used an Nd:YAG (532 nm) pumped dye-laser system as the laser source. The short pulse (∼ 25 ns), high repetition rate (∼ 8.5 kHz) 308 nm laser used for fluorescence

excitation was obtained by frequency doubling the 616 nm laser output of the dye-laser. The fluorescence signal is determined by a range of instrumental parameters and regular on-site calibration is required. The DOAS instrument used an ultra-violet (UV) laser at 308.04 nm with a bandwidth of ∼ 0.5 nm as the probe light. The laser system is a picosecond (ps) mode-locked Nd:YAG laser pumped dye laser system with a pulse duration of 800 femtosecond (fs). Only one instrument, installed in the SAPHIR chamber in Jülich, Germany, is still in operation. The concentration of OH can be directly retrieved from the broad-band absorption spectral obtained from a grating monochromator, and the direct absorption measurement is inherently calibration free [3].

The UV laser systems currently used in FAGE and DOAS instruments are expensive, bulky, and complex. Therefore, attempts have been made to develop continuous-wave (CW) tunable UV laser based on sum frequency generation or second harmonic generation with diode lasers [4–6]. But output powers were low, ranging from picowatt (pW) to nanowatt (nW), and limiting the application to long-path measurements.

The rapid development of diode laser technology has brought new opportunities for laser spectroscopy and even changed traditional spectroscopy methods. Especially in the mid-infrared (MIR) region, the fundamental vibrational band with strong absorption intensity makes it a good choice for high-sensitivity detection [7–9]. Compared to UV laser spectroscopy, diode lasers are small, low cost, easy to use and more convenient. It provides better wavelength resolution and selectivity than UV spectroscopy.

Recently, we demonstrated OH detection with Faraday rotation spectroscopy (FRS) using a distributed feed-back (DFB) diode laser operating at 2.8 μm [10,11]. The $Q(1.5)$ double lines at ∼ 3568 cm^{-1} have strong absorption line intensities (∼ 9×10^{-20} cm^{-1}/(molecule cm^{-2}) at room temperature) [12], making it a good choice for high-sensitivity OH detection in the infrared spectral region. By coupling a multipass cell to FRS, a detection limit of 1.6×10^6 molecule/cm^3 (1σ, 4s) was achieved in a simulation chamber with an effective absorption pathlength of 108 m [13]. On this basis, a laser-flash photolysis instrument for the total OH reactivity measurement was developed [14]. A detection limit of 1.1×10^7 molecule/cm^3 (1σ, 8s) was achieved with an effective absorption pathlength of 25 m. To further improve the detection limit, increasing the effective absorption pathlength is a first step.

In this work, cavity-enhanced method was used. An optical-feedback cavity-enhanced absorption spectroscopy (OF-CEAS) approach using a 2.8 μm DFB diode laser is implemented for OH detection. Optical feedback (OF) is a unique property of diode lasers, where a reflector outside the laser cavity reflects a small fraction of the laser output back into the laser cavity, enables optical self-locking system with high spectral purity [15–17]. OF from a high-finesse Fabry-Perot cavity can drastically reduce the laser linewidth and tightly lock the laser frequency to the cavity resonance, significantly reducing the laser phase and amplitude noise, thus enabling efficient injection of the laser into narrow cavity modes to achieve strong and stable cavity transmission [18–21]. These advantages make OF-CEAS [22] a simple and sensitive detection technique, which has been successfully used in various applications [21], such as isotope measurement on high-altitude aircraft [23], volcanic emission measurement [24], and ambient trace gases detection [25–27]. The typical detection sensitivity of OF-CEAS systems was ∼ 5×10^{-10} cm^{-1} with 1 s data averaging time for a cavity of ∼ 20 μs ring-down time (τ_0) [22]. By combining optical feedback and frequency stabilized cavity ring-down spectroscopy (OF-FS-CRDS), a near-shot-noise-limit of 1.9×10^{-13} cm^{-1} can be achieved with an integration time of 20 s and a τ_0 of ∼ 150 μs [28]. Lessons from shot-noise-level birefringence phase shift measurement show the potential of using OF-CEAS in combination with other high-sensitivity approaches for high-sensitivity OH detection [29].

2. Experimental section

The experimental set-up of the OF-CEAS instrument for OH detection is schematically shown in Fig. 1. The V-shaped cavity and the optical breadboard were made of hard aluminum alloy with high strength. The two arms of the V-shaped cavity were of equal length, both 48.8 cm, at an angle of 6° to each other, giving a free spectral range (FSR) of 153.7 MHz. The high reflectivity mirrors (M0-M2, LGR, 1 in. diameter, 1 m radius of curvature) were installed in the mirror chambers at both ends of the cavity, sealed with three 1 in. diameter AR-coated (from 1.65 to 3.0 μm) ZnSe wedged windows (Thorlabs WW71050-D). When necessary, the chambers can be continuously flushed with high-purity nitrogen or zero air to prevent mirror reflectivity degradation. The volume of the V-shaped cavity was about 1 L. Three 254 nm UV lamps (Analytikjena) were installed on the top of the cavity for the photolysis of O_3 to generate OH radical samples [14]. The flow rate of the sample was controlled by a mass flow meter. The pressure of the cavity was monitored and controlled with a vacuum gauge (Pfeiffer CCR361) and an electric butterfly valve (VAT DN40KF).
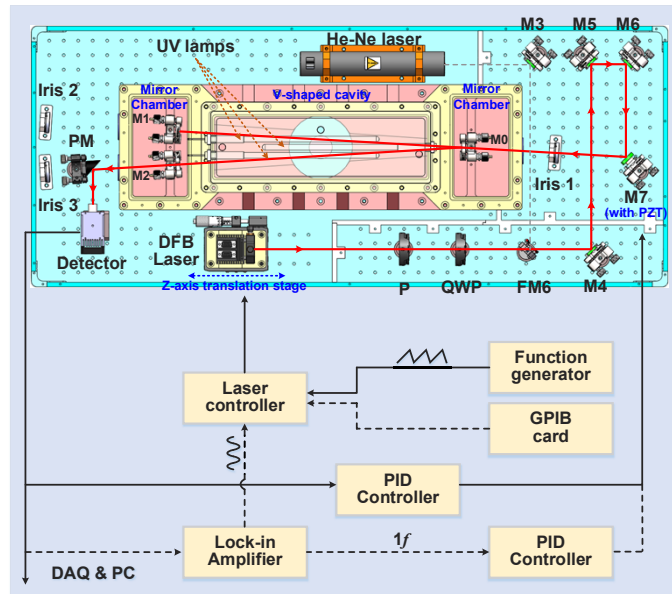

Fig. 1. Schematic diagram of the OF-CEAS system. P: Rochon polarizer; QWP: quarter-wave plate; FM: foldable mirror; M0-M2: high reflectivity mirrors; M4-M7: protected silver mirrors; PM: parabolic mirror; DAQ: data acquisition; PC: personal computer.

The laser light source was a 2.8 μm CW DFB (TO5 header with cubic mount, Nanoplus GmbH) diode laser operating at room temperature, controlled by an LDC501 controller (Stanford Research). The tuning of the laser frequency can be realized by scanning the laser injection current with a ramp generated by a function generator or by controlling the injection current step-by-step via a GPIB card. The collimated output of the laser was passed through a Rochon polarizer (Foctek Photonics), a quarter-wave plate (QWP, MT Optics, center wavelength at 2.796 μm), four mirrors (M4-M7), and then injected into the cavity. Light emerging from the cavity mirror M2 was focused by a 90° off-axis parabolic mirror (silver coated, with an effective focal length of 50.8 mm) onto a thermoelectrically cooled (HgCdZn)Te photovoltaic detector (Vigo PVI-4TE-3.4). A He-Ne laser was used for optical alignment. Fast switching between the red light and infrared light paths was achieved by using a flipper optical mount (FM6).

The optical feedback rate (β) of the laser was controlled by rotating the QWP. For DFB lasers, the optimal value of β is $\sim 10^{-4}$-10^{-5} [17]. The advantage of the V-shaped cavity is that it avoids the optical feedback of the light directly reflected by the input high reflectivity mirror of the cavity. Optical feedback rates much smaller than a few percent are easy to access.

To keep the feedback phase in an optimum condition, the laser-to-cavity distance needs to be controlled an odd multiple of the cavity arm. In this work, the laser was mounted on a compact translation stage. First, the distance between the laser to the cavity mirror M0 was coarsely adjusted to approximately 3 times the length of the cavity arm. Then, fine distance adjustment to control the phase of the OF was made via the PZT mounted on the steering mirror M7. An electronic servo loop (SIM960 analog PID controller, Stanford) maintained the correct phase of the feedback for laser injection and locking of the laser frequency to the cavity mode. The error signal can be derived by the symmetry analysis of the cavity mode (symmetry analysis method) [22,30,31] or by the first harmonic ($1f$) obtained by laser injection current modulation and phase sensitive detection with a lock-in amplifier (wavelength modulation method) [32].

3. Results

3.1. Principle of the optical feedback for a V-shaped cavity

In the case of weak feedback, the relationships between the free running laser frequency (ω_{free}) and the coupled laser frequency ($\omega = 2\pi c/\lambda$) for a V-shaped cavity is given by [17,22]:

$$\omega_{free} = \omega + K \frac{\sin\left[\frac{2\omega}{c}(L_0 + L_1) + \theta\right] - R^2 \sin\left[\frac{2\omega}{c}(L_0 - L_2) + \theta\right]}{1 + \left(\frac{2R}{1-R^2}\right)^2 \sin^2\left[\frac{\omega}{c}(L_1 + L_2)\right]} \tag{1}$$

where L_0 is the distance from the output laser facet to the high reflectivity mirror M0. L_1 and L_2 are the lengths of the two arms of the V-cavity. R is the mirror reflectivity of the cavity (for simplicity, assume the reflectivity of the three mirrors are the same.). $\theta = \arctan\alpha$ is related to the gain response to the laser, where α is the phase amplitude coupling factor or Henry factor. The value of the constant K is given by:

$$K = \sqrt{\beta(1 + \alpha^2)} \frac{c}{2n_0 L_d} \frac{F_C}{2F_d} \tag{2}$$

where n_0 and L_d are the optical index (in the absence of carriers) and the length of the laser cavity, respectively. F_c and F_d are the finesses of V-cavity and diode laser cavity ($F_c = \frac{\pi R}{1-R^2}$, $F_d = \frac{\pi \sqrt{R_d}}{1-R_d}$, R_d is the reflectivity of the diode laser facet). The propagation term $2\omega(L_0 + L_1)/c$, known as OF phase (ϕ), can be adjusted by changing the distance of L_0. For a favorable condition of $\phi = -\theta$, the transmission profile will be around the top of the cavity resonance [21,22].

A simulation of the cavity transmission signal and corresponding coupled frequency as a function of free running frequency are shown in Fig. 2. Within the locking range, the laser remains locked to the cavity resonance. The tuning speed of the laser is greatly reduced (about 1000 times here), and the coupled laser only be tuned over a small spectral region ($\sim$ 100 kHz) within the resonance profile. A stable and broad transmission profile is observed. When the locking range is adjusted to be close to the cavity free spectral range (FSR), the laser jumps from one longitudinal cavity mode to the next, achieving "automatic mode matching" [22]. The absorption spectrum thus can be obtained by recording the maxima of the successive cavity mode profiles.

3.2. Symmetry analysis method

A typical cavity transmission of OF-CEAS system is shown in Fig. 3. The laser injection current was driven by a 50 Hz voltage ramp across 30 cavity modes ($\sim$ 0.15 cm^{-1}). One of the modes
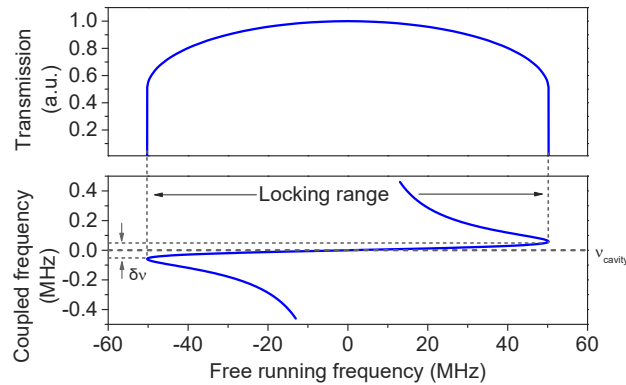
Fig. 2. Simulation of (a) the cavity transmission signal and (b) the corresponding coupled laser frequency as a function of free running laser frequency.

was selected for the symmetry analysis. Using a custom-written program, the cavity mode was divided into left and right parts (A and B, as shown in the right panel of Fig. 3) according to the peak value of the cavity mode. The areas of these two parts were calculated. The difference of the two areas was fed to the PID controller as an error signal to precisely control the expansion and contraction of the PZT mounted on mirror M7, thereby fine-tuning the distance between the laser and the cavity to maintain the phase matching. When the M7 was located at the optimal position (with the correct OF phase), the difference between the areas of the left and right parts was zero and the shape of the cavity mode was symmetrical. In this case, the laser frequency was locked to the cavity resonance, which greatly improved the coupling efficiency, resulting in a stable, broad, and symmetric-looking transmission profile.
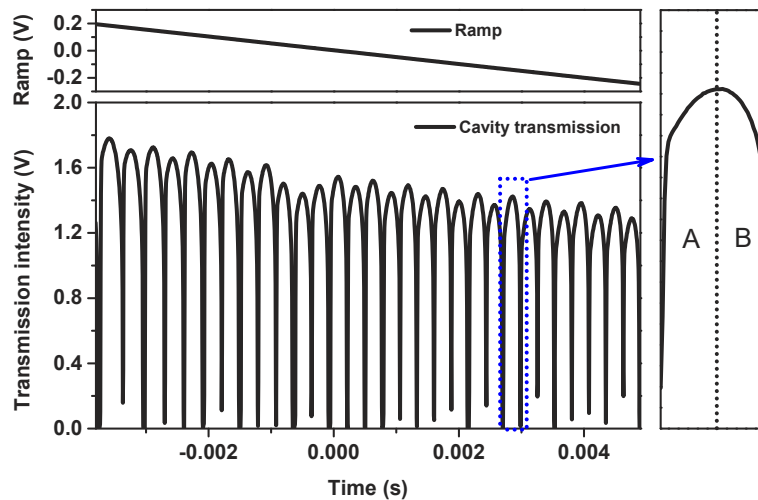

Fig. 3. On the left is the cavity transmission signal as a function of time recorded by applying a linear current ramp to the diode laser injection current. On the right is a zoomed-in profile showing the cavity mode. The dotted line indicates the peak position, dividing the cavity mode into left (A) and right (B) parts.

   The absorption of the molecule can be easily obtained by using a peak picking algorithm to find the maximum cavity transmission intensity of each cavity mode [33]. The group of these
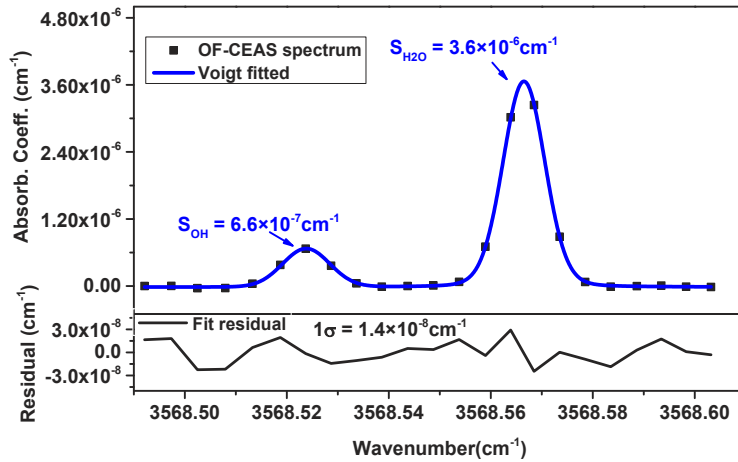
Fig. 4. Absorption spectra of OH and H_2O measured with a 2 s acquisition time at 50 Hz scan rate (100-sweep average). A fitted Voigt profile and the corresponding fitting residual are presented.

maxima intensities and cavity mode number produced the frequency-dependent spectrum of transmitted intensity $I(\nu)$. The absorption coefficient $\alpha(\nu)$ can be written in the form [25,34, 35]:

$$\alpha = \frac{1}{d}\left(\sqrt{\frac{I_0}{I}} - 1\right)(1 - R) \tag{3}$$

where I_0 is the light intensity transmitted through the cavity without absorber and can be deduced from the polynomial fit of the baseline. d is the sum of the two arms of the V-cavity and equals to 97.6 cm. R is mirror reflectivity, which was determined by measuring the integrated absorption $\sqrt{I_0/I}/d$ with known concentration of CO_2 [36,37]. In this work, R was determined to be 0.9988, giving a ring-down time of 1.4 µs and an effective absorption pathlength [$L_{eff} = d/(1-R)$] of 823 m.

Examples of OF-CEAS spectra of OH at 3568.52 cm^{-1} and H_2O at 3567.57 cm^{-1} with 2 s acquisition time (50 Hz ramp, 100-sweep average) at 10 mbar pressure are shown in Fig. 4. A Voigt line profile was used to fit the experimental data with Levenberg–Marquardt non-linear least square method. The OH concentration was determined to be 8.7×10^{10} molecule/cm^3. With a fit residual of 1.4×10^{-8} cm^{-1} and the peak absorption of OH radical (S_{OH}) of 6.6×10^{-7} cm^{-1}, a 1σ detection limit of 1.8×10^9 molecule/cm^3 was achieved.

Time series measurement was performed to investigate the stability and precision of the 2.8 µm OF-CEAS system with the symmetry analysis method. One cavity mode of the absorption baseline was chosen to get the continuous measurement of the absorption coefficient in Fig. 5. The Allan variance analysis is shown in the lower panel. The detection sensitivity can be further improved to 5.5×10^{-9} cm^{-1} with an average time of 16 s, giving an OH detection limit of ~ 7.2×10^8 molecule/cm^3.

3.3. *Wavelength modulation method*

In the symmetry analysis method, the laser was periodically locked to the cavity mode. Loss of lock occurs as the laser is swept through different cavity modes. To reduce the duty cycle caused by the laser decoupling from the cavity, the wavelength modulation method was developed. Here, the laser injection current was firstly modulated by adding a sinusoidal wave with a frequency of 31 kHz and an amplitude of 14 mV onto a ramp. The modulated cavity mode transmission is

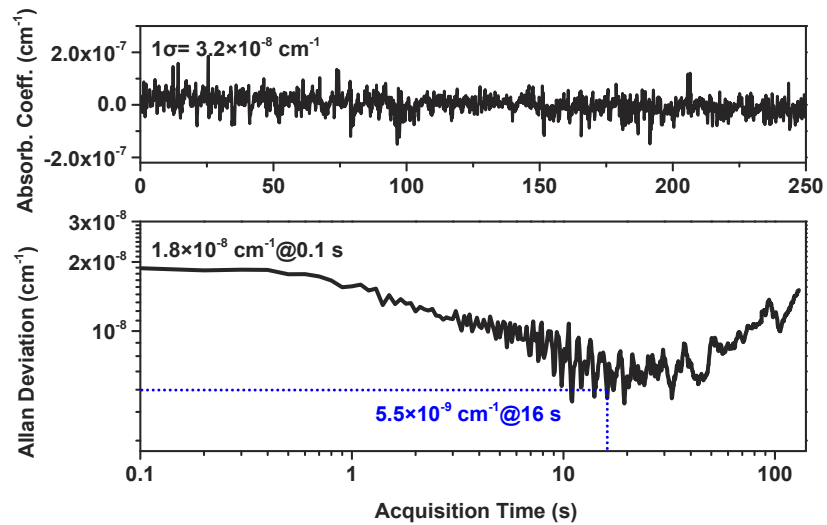**Fig. 5.** Performance evaluation of the OF-CEAS instrument. Upper panel: time series measurement of absorption coefficient for a cavity mode on the absorption baseline. Lower panel: Allan deviation plot.
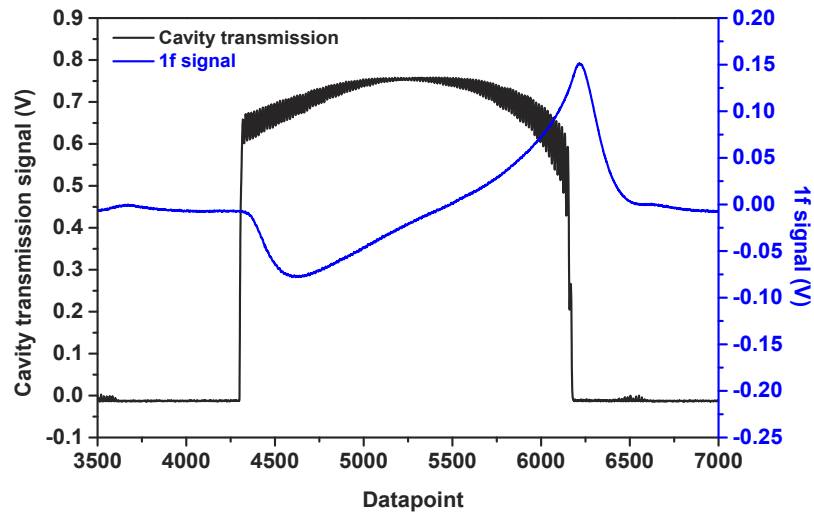

Fig. 6. Modulated cavity mode transmission and the corresponding $1f$ signal of a cavity mode with 10 kHz filter from a lock-in amplifier. The $1f$ signal provides an error signal to the PID controller.

shown in Fig. 6. The corresponding $1f$ signal of the cavity mode demodulated by the lock-in amplifier was used as an error signal and was sent to the PID controller to control the OF phase.

There is a zero-crossing in the $1f$ signal, which corresponds to the maximum of the cavity transmission. When the laser center frequency was set in the locking range and a symmetric-looking transmission profile was observed, the ramp in the modulation was removed. At this time, the amplitude of the sinusoidal wave was gradually reduced. When the amplitude is reduced to 4 mV (corresponding to a modulation depth of about 8 MHz), the small distortion of the laser led to a small change ($\sim 1\%$) in the transmission intensity. The laser frequency was locked to the maximum transition and the system worked stably [32].

In this case, the laser worked as an optically self-locked laser. Automatic mode matching was achieved. The laser frequency was tuned using a GPIB card and was continuously locked to the center of a cavity mode, thus keeping the transmitted light intensity of the OF-CEAS system at a maximum value. For free radical detection, it is usually not necessary to scan the entire absorption spectrum, but instead fix the laser frequency at the peak absorption of OH radical. In this case, continuously locking the laser frequency to the cavity mode without scanning the laser will show its advantage.

Figure 7 shows the time series measurement of the empty cavity at a fixed wavelength with wavelength modulation method. The Allan variance shows that the detection sensitivity can be further improved to 1.7×10^{-9} cm^{-1} with an average time of 25 s, which was about 3 times better than the symmetrical method. The corresponding OH detection limit was $\sim 2 \times 10^8$ molecule/cm^3.
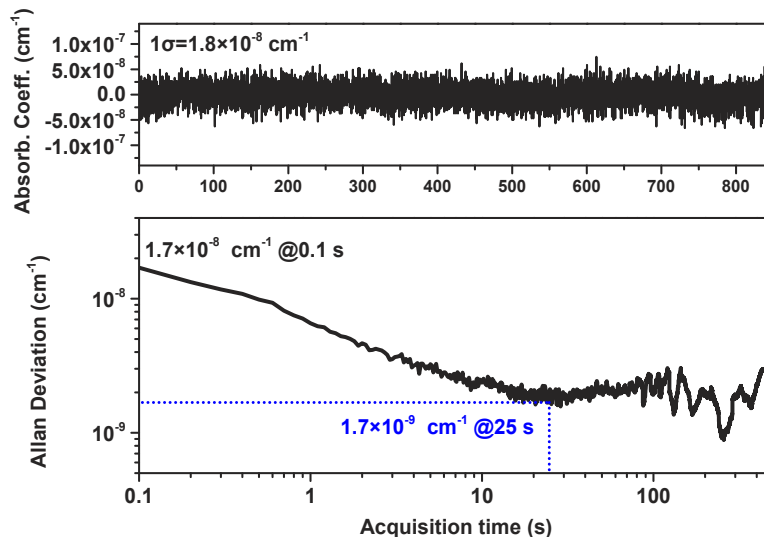

Fig. 7. Performance evaluation of the OF-CEAS system with injection current modulation and phase sensitive detection. Upper panel: time series measurement. Lower panel: Allan deviation plot.

A comparison of the detection sensitivity with some literature reported V-shaped OF-CEAS instruments is shown in Table 1. The reported mid-infrared OF-CEAS systems are mainly based on interband cascade lasers (ICL) and quantum cascade lasers (QCL). In recent years, some applications of DFB lasers in the mid-infrared spectral region have also been reported. With the cavity finesse ranging from 1880 to 144000, the reported detection sensitivity ranged from 7.1×10^{-8} cm^{-1} to 8×10^{-11} cm^{-1} with a data acquisition time from 0.1 s to 50 s. The detection sensitivity of our instrument was $\sim 1.7 \times 10^{-9}$ cm^{-1} with an effective absorption pathlength of 823 m. The corresponding minimal detectable fractional absorption ($\Delta\alpha \times L_{eff}$) reported here was

about 1×10^{-4}, which was compared to that achieved with longer L_{eff}. The 2.8 µm OF-CEAS system reported here has good performance under current conditions. Due to the lower mirror reflectivity used here, the effective absorption pathlength was relatively low. By replacing mirrors with higher reflectivity, higher detection sensitivity will be obtained.

Table 1. Performance comparison of the V-shaped OF-CEAS instruments

Light Source	Wavelength (µm)	Species	Cavity Finesse	Mirror Reflectivity	Cavity Length (m)	Effective Absorption Pathlength (km)	Data acquisition time (s)	Detection Sensitivity (cm^{-1})	Minimal detectable fractional absorption	Reference
ECDL	0.44	NO_2	17000	0.99991	99.2	10	0.1	3.5×10^{-9}	3.5×10^{-3}	[38]
VECSEL	2.33	$H_2^{18}O$, $H_2^{17}O$, HDO	144000	0.999989	97.8	90	0.5	8×10^{-11}	7.2×10^{-4}	[39]
ICL	3.24	CH_4	1880	0.99917	80	0.96	2	7.1×10^{-8}	6.8×10^{-3}	[34]
	3.3	C_2H_6, CH_4, $\delta^{13}C$-CH_4	3800	0.999584	80	1	0.1	2.8×10^{-9}	2.8×10^{-4}	[26]
	3.29	NO_2	1500	0.9989	100	5	0.1	1.5×10^{-8}	7.5×10^{-3}	[35]
	5.3	NO	11400	0.99986	80	5.8	0.2	1.3×10^{-9}	7.5×10^{-4}	[40]
QCL	4.46	N_2O	7850	0.9998	100	5	1	3×10^{-9}	1.5×10^{-3}	[18]
	5.26	NO	6200	0.99975	99	4	0.1	2×10^{-9}	8×10^{-4}	[41]
	5.6	H_2CO	10000	0.99985	98	6.3	0.1	1.6×10^{-9}	1×10^{-3}	[42]
	7.39	CH_4	5400	0.9997	80	2.76	50	5.3×10^{-10}	1.5×10^{-4}	[25]
	7.84	CH_4, N_2O	9000	0.999652	72.7	2.1	1	5.5×10^{-8}	1.1×10^{-2}	[43]
DFB	1.31	HF	20000	0.99992	88	5	0.1	2×10^{-9}	1×10^{-3}	[22]
	1.39	$\delta^{18}O$, $\delta^{17}O$, $\delta^{2}H$,	20000	0.99992	106	15	1	4×10^{-10}	6×10^{-4}	[23]
	1.59	$^{13}CO_2$, $^{12}CO_2$	3500	0.9991	149	1.7	2	4.07×10^{-9}	6.9×10^{-4}	[31]
	1.6	CO_2	24000	0.99993	88	13.5	4	5×10^{-10}	6.8×10^{-4}	[44]
	1.65	CH_4	17500	0.99991	85	9.5	0.2	2×10^{-9}	1.9×10^{-3}	[45]
	2.33	CH_4, CO_2	15700	0.9999	100	10	0.1	$\sim 10^{-8}$	$\sim 10^{-2}$	[24]
	2.33	CO, CH_4, NH_3	30000	0.99995	100	19	0.3	3×10^{-10}	5.7×10^{-4}	[46]
	2.8	**OH**	**1300**	**0.9988**	**97.6**	**0.8**	**25**	**1.7×10^{-9}**	**1.4×10^{-4}**	**This work**

4. Conclusion

We report the development of an OF-CEAS instrument with 2.8 µm DFB diode laser for OH radical detection. Two different phase control approaches were used to achieve laser locking to the cavity mode. The first method used a 50 Hz ramp voltage to drive the laser injection current, which crossed dozens of cavity modes in one scan. One of the cavity modes was used for the symmetry analysis. By comparing the shape, an error signal was generated and was fed to a PID controller. A detection limit of 5.5×10^{-9} cm^{-1} was achieved with an integration time of 16 s, giving an OH detection limit of $\sim 7.2 \times 10^{8}$ molecule/cm^3. The second method used injection current modulation (with 31 kHz sine wave) and phase sensitive detection to continuously lock the laser frequency to a cavity mode. The detection sensitivity was improved to 1.7×10^{-9} cm^{-1} (with 25 s integration time). The corresponding OH detection limit was improved to $\sim 2 \times 10^{8}$ molecule/cm^3. We expect higher sensitivity to be obtained by using higher reflectivity mirrors. Taking advantages of optically self-locking property of optical feedback, combined with other modulation spectroscopy methods, such as frequency modulation spectroscopy (FMS) [47] and

Faraday rotation spectroscopy (FRS) [13], the modulated OF-CEAS instrument may achieve shot-noise limited detection [28,29].

Disclosures. The authors declare no conflicts of interest.

Data availability. Data underlying the results presented in this paper are not publicly available at this time but may be obtained from the authors upon reasonable request.

References

1. D. E. Heard and M. J. Pilling, "Measurement of OH and HO_2 in the troposphere," Chem. Rev. **103**(12), 5163–5198 (2003).
2. K. Lu, S. Guo, Z. Tan, H. Wang, D. Shang, Y. Liu, X. Li, Z. Wu, M. Hu, and Y. Zhang, "Exploring atmospheric free-radical chemistry in China: the self-cleansing capacity and the formation of secondary air pollution," Natl. Sci. Rev. **6**(3), 579–594 (2019).
3. H. Fuchs, H. P. Dorn, M. Bachner, B. Bohn, T. Brauers, S. Gomm, A. Hofzumahaus, F. Holland, S. Nehr, F. Rohrer, R. Tillmann, and A. Wahner, "Comparison of OH concentration measurements by DOAS and LIF during SAPHIR chamber experiments at high OH reactivity and low NO concentration," Atmos. Meas. Tech. **5**(7), 1611–1626 (2012).
4. G. Hancock and V. L. Kasyutich, "UV cavity enhanced absorption spectroscopy of the hydroxyl radical," Appl. Phys. B **79**(3), 383–388 (2004).
5. L. Corner, J. S. Gibb, G. Hancock, A. Hutchinson, V. L. Kasyutich, R. Peverall, and G. A. D. Ritchie, "Sum frequency generation at 309 nm using a violet and a near-IR DFB diode laser for detection of OH," Appl. Phys. B **74**(4-5), 441–444 (2002).
6. H. R. Barry, B. Bakowski, L. Corner, T. Freegarde, O. T. W. Hawkins, G. Hancock, R. M. J. Jacobs, R. Peverall, and G. A. D. Ritchie, "OH detection by absorption of frequency-doubled diode laser radiation at 308 nm," Chem. Phys. Lett. **319**(1-2), 125–130 (2000).
7. G. Pesce, G. Rusciano, and A. Sasso, "Detection and spectroscopy of OH fundamental vibrational band based on a difference frequency generator at 3 µm," Chem. Phys. Lett. **374**(5-6), 425–431 (2003).
8. S. Schilt, F. K. Tittel, and K. P. Petrov, "Diode laser spectroscopic monitoring of trace gases," Encyclopedia of Analytical Chemistry 1-29 (2011).
9. W. Chen, H. Yi, T. Wu, W. Zhao, C. Lengignon, G. Wang, E. Fertein, C. Coeur, G. Wysocki, T. Wang, M.W. Sigrist, X. Gao, and W. Zhang, "Photonic sensing of reactive atmospheric species," in: R.A. Meyers (Eds.), *Encyclopedia of Analytical Chemistry*, © 2017, John Wiley & Sons, Ltd. doi: 10.1002/9780470027318.a9432.
10. W. Zhao, G. Wysocki, W. Chen, E. Fertein, D. Le Coq, D. Petitprez, and W. Zhang, "Sensitive and selective detection of OH radicals using Faraday rotation spectroscopy at 2.8 µm," Opt. Express **19**(3), 2493–2501 (2011).
11. W. Zhao, G. Wysocki, W. Chen, and W. Zhang, "High sensitivity Faraday rotation spectrometer for hydroxyl radical detection at 2.8 µm," Appl. Phys. B **109**(3), 511–519 (2012).
12. I. E. Gordon, L. S. Rothman, R. J. Hargreaves, R. Hashemi, E. V. Karlovets, F. M. Skinner, E. K. Conway, C. Hill, R. V. Kochanov, Y. Tan, P. Wcisło, A. A. Finenko, K. Nelson, P. F. Bernath, M. Birk, V. Boudon, A. Campargue, K. V. Chance, A. Coustenis, B. J. Drouin, J. M. Flaud, R. R. Gamache, J. T. Hodges, D. Jacquemart, E. J. Mlawer, A. V. Nikitin, V. I. Perevalov, M. Rotger, J. Tennyson, G. C. Toon, H. Tran, V. G. Tyuterev, E. M. Adkins, A. Baker, A. Barbe, E. Canè, A. G. Császár, A. Dudaryonok, O. Egorov, A. J. Fleisher, H. Fleurbaey, A. Foltynowicz, T. Furtenbacher, J. J. Harrison, J. M. Hartmann, V. M. Horneman, X. Huang, T. Karman, J. Karns, S. Kassi, I. Kleiner, V. Kofman, F. Kwabia-Tchana, N. N. Lavrentieva, T. J. Lee, D. A. Long, A. A. Lukashevskaya, O. M. Lyulin, V. Y. Makhnev, W. Matt, S. T. Massie, M. Melosso, S. N. Mikhailenko, D. Mondelain, H. S. P. Müller, O. V. Naumenko, A. Perrin, O. L. Polyansky, E. Raddaoui, P. L. Raston, Z. D. Reed, M. Rey, C. Richard, R. Tóbiás, I. Sadiek, D. W. Schwenke, E. Starikova, K. Sung, F. Tamassia, S. A. Tashkun, J. V. Auwera, I. A. Vasilenko, A. A. Vigasin, G. L. Villanueva, B. Vispoel, G. Wagner, A. Yachmenev, and S. N. Yurchenko, "The HITRAN2020 molecular spectroscopic database," J. Quant. Spectrosc. Radiat. Transfer **277**, 107949 (2022).
13. W. Zhao, B. Fang, X. Lin, Y. Gai, W. Zhang, W. Chen, Z. Chen, H. Zhang, and W. Chen, "Superconducting-magnet-based Faraday rotation spectrometer for real time in-situ measurement of OH radicals at 10^6 molecule/cm³ level in an atmospheric simulation chamber," Anal. Chem. **90**(6), 3958–3964 (2018).
14. N. Wei, B. Fang, W. Zhao, C. Wang, N. Yang, W. Zhang, W. Chen, and C. Fittschen, "Time-resolved laser-flash photolysis Faraday rotation spectrometer: a new tool for total OH reactivity measurement and free radical kinetics research," Anal. Chem. **92**(6), 4334–4339 (2020).
15. R. Lang and K. Kobayashi, "External optical feedback effects on semiconductor injection laser properties," IEEE J. Quantum. Electron. **16**(3), 347–355 (1980).
16. B. Dahmani, L. Hollberg, and R. Drullinger, "Frequency stabilization of semiconductor lasers by resonant optical feedback," Opt. Lett. **12**(11), 876–878 (1987).

17. P. Laurent, A. Clairon, and C. Breant, "Frequency noise analysis of optically self-locked diode lasers," IEEE J. Quantum. Electron. **25**(6), 1131–1142 (1989).

18. G. Maisons, P. G. Carbajo, M. Carras, and D. Romanini, "Optical-feedback cavity-enhanced absorption spectroscopy with a quantum cascade laser," Opt. Lett. **35**(21), 3607–3609 (2010).

19. E. Fasci, N. Coluccelli, M. Cassinerio, A. Gambetta, L. Hilico, L. Gianfrani, P. Laporta, A. Castrillo, and G. Galzerano, "Narrow-linewidth quantum cascade laser at 8.6 µm," Opt. Lett. **39**(16), 4946–4949 (2014).

20. G. Zhao, J. Tian, J. T. Hodges, and A. J. Fleisher, "Frequency stabilization of a quantum cascade laser by weak resonant feedback from a Fabry-Perot cavity," Opt. Lett. **46**(13), 3057–3060 (2021).

21. J. Morville, D. Romanini, and E. Kerstel, "Cavity enhanced absorption spectroscopy with optical feedback," in *Cavity-Enhanced Spectroscopy and Sensing*, G. Gagliardi and H. P. Loock, eds. (Springer, 2014), pp. 163–209.

22. J. Morville, S. Kassi, M. Chenevier, and D. Romanini, "Fast, low-noise, mode-by-mode, cavity-enhanced absorption spectroscopy by diode-laser self-locking," Appl. Phys. B **80**(8), 1027–1038 (2005).

23. E. R. T. Kerstel, R. Q. Iannone, M. Chenevier, S. Kassi, H.-J. Jost, and D. Romanini, "A water isotope (^{2}H, ^{17}O, and ^{18}O) spectrometer based on optical feedback cavity-enhanced absorption for in situ airborne applications," Appl. Phys. B **85**(2-3), 397–406 (2006).

24. S. Kassi, M. Chenevier, L. Gianfrani, A. Salhi, Y. Rouillard, A. Ouvrard, and D. Romanini, "Looking into the volcano with a Mid-IR DFB diode laser and Cavity Enhanced Absorption Spectroscopy," Opt. Express **14**(23), 11442–11452 (2006).

25. N. Lang, U. Macherius, M. Wiese, H. Zimmermann, J. Röpcke, and J. H. van Helden, "Sensitive CH_4 detection applying quantum cascade laser based optical feedback cavity-enhanced absorption spectroscopy," Opt. Express **24**(6), A536–A543 (2016).

26. L. Lechevallier, R. Grilli, E. Kerstel, D. Romanini, and J. Chappellaz, "Simultaneous detection of C_2H_6, CH_4, and δ^{13}C-CH_4 using optical feedback cavity-enhanced absorption spectroscopy in the mid-infrared region: towards application for dissolved gas measurements," Atmos. Meas. Tech. **12**(6), 3101–3109 (2019).

27. J. Tian, G. Zhao, A. J. Fleisher, W. Ma, and S. Jia, "Optical feedback linear cavity enhanced absorption spectroscopy," Opt. Express **29**(17), 26831–26840 (2021).

28. J. Burkart, D. Romanini, and S. Kassi, "Optical feedback frequency stabilized cavity ring-down spectroscopy," Opt. Lett. **39**(16), 4695–4698 (2014).

29. M. Durand, J. Morville, and D. Romanini, "Shot-noise-limited measurement of sub-parts-per-trillion birefringence phase shift in a high-finesse cavity," Phys. Rev. A **82**(3), 031803 (2010).

30. A. G. V. Bergin, G. Hancock, G. A. D. Ritchie, and D. Weidmann, "Linear cavity optical-feedback cavity-enhanced absorption spectroscopy with a quantum cascade laser," Opt. Lett. **38**(14), 2475–2477 (2013).

31. S. G. Baran, G. Hancock, R. Peverall, G. A. D. Ritchie, and N. J. van Leeuwen, "Optical feedback cavity enhanced absorption spectroscopy with diode lasers," Analyst **134**(2), 243–249 (2009).

32. S. Ohshirpa and H. Schnatz, "Optimization of injection current and feedback phase of an optically self-locked laser diode," J. Appl. Phys. **71**(7), 3114–3117 (1992).

33. D. J. Hamilton, M. G. D. Nix, S. G. Baran, G. Hancock, and A. J. Orr-Ewing, "Optical feedback cavity-enhanced absorption spectroscopy (OF-CEAS) in a ring cavity," Appl. Phys. B **100**(2), 233–242 (2010).

34. K. M. Manfred, G. A. D. Ritchie, N. Lang, J. Ropcke, and J. H. van Helden, "Optical feedback cavity-enhanced absorption spectroscopy with a 3.24 µm interband cascade laser," Appl. Phys. Lett. **106**(22), 221106 (2015).

35. K. M. Manfred, K. M. Hunter, L. Ciaffoni, and G. A. D. Ritchie, "ICL-based OF-CEAS: a sensitive tool for analytical chemistry," Anal. Chem. **89**(1), 902–909 (2017).

36. W. Zhao, X. Gao, W. Chen, W. Zhang, T. Huang, T. Wu, and H. Cha, "Wavelength modulated off-axis integrated cavity output spectroscopy in the near infrared," Appl. Phys. B **86**(2), 353–359 (2007).

37. W. Zhao, X. Gao, L. Deng, T. Huang, T. Wu, and W. Zhang, "Absorption spectroscopy of formaldehyde at 1.573 µm," J. Quant. Spectrosc. Radiat. Transfer **107**(2), 331–339 (2007).

38. I. Courtillot, J. Morville, V. Motto-ros, and D. Romanini, "Sub-ppb NO_2 detection by optical feedback cavity-enhanced absorption spectroscopy with a blue diode laser," Appl. Phys. B **85**(2-3), 407–412 (2006).

39. J. Landsberg, D. Romanini, and E. Kerstel, "Very high finesse optical-feedback cavity-enhanced absorption spectrometer for low concentration water vapor isotope analyses," Opt. Lett. **39**(7), 1795–1798 (2014).

40. L. Richard, D. Romanini, and I. Ventrillard, "Nitric oxide analysis down to ppt levels by optical-feedback cavity-enhanced absorption spectroscopy," Sensors **18**(7), 1997 (2018).

41. I. Ventrillard, P. G. Carbajo, and D. Romanini, "Part per trillion nitric oxide measurement by optical feedback cavity-enhanced absorption spectroscopy in the mid-infrared," Appl. Phys. B **123**(6), 180 (2017).

42. P. G. Carbajo, E. Fasci, I. Ventrillard, M. Carras, G. Maisons, and D. Romanini, "Optical-feedback cavity-enhanced absorption spectroscopy with a quantum-cascade laser yields the lowest formaldehyde detection limit," Appl. Phys. B **110**(3), 309–314 (2013).

43. D. J. Hamilton and A. J. Orr-Ewing, "A quantum cascade laser-based optical feedback cavity-enhanced absorption spectrometer for the simultaneous measurement of CH_4 and N_2O in air," Appl. Phys. B **102**(4), 879–890 (2011).

44. T. Desbois, I. Ventrillard, and D. Romanini, "Simultaneous cavity-enhanced and cavity ringdown absorption spectroscopy using optical feedback," Appl. Phys. B **116**(1), 195–201 (2014).

45. D. Romanini, M. Chenevier, S. Kassi, M. Schmidt, C. Valant, M. Ramonet, J. Lopez, and H.-J. Jost, "Optical–feedback cavity–enhanced absorption: a compact spectrometer for real–time measurement of atmospheric methane," Appl. Phys. B **83**(4), 659–667 (2006).

46. I. Ventrillard-Courtillot, T. Gonthiez, C. Clerici, and D. Romanini, "Multispecies breath analysis faster than a single respiratory cycle by optical-feedback cavity-enhanced absorption spectroscopy," J. Bio. Opt. **14**(6), 064026 (2009).
47. V. L. Kasyutich and M. W. Sigrist, "Characterisation of the potential of frequency modulation and optical feedback locking for cavity-enhanced absorption spectroscopy," Appl. Phys. B **111**(3), 341–349 (2013).